Available online at www.sciencedirect.com

SciVerse ScienceDirect

Ceramics International 39 (2013) 5263–5270

CERAMICS INTERNATIONAL

www.elsevier.com/locate/ceramint

Electrochemical behavior of $La_{0.8}Sr_{0.2}FeO_3$ electrode with different porosities under cathodic and anodic polarization

Jing Wang*, Yong Zhang, Wenli Guo, Xiangyuan Hou, Tongxiang Liang, Changsheng Deng*, Jingming Xu

Beijing Fine Ceramics Laboratory, State Key Laboratory of New Ceramics and Fine Processing, Institute of Nuclear and New Energy Technology, Tsinghua University, Beijing 100084, PR China

Received 3 October 2012; received in revised form 9 December 2012; accepted 9 December 2012
Available online 20 December 2012

Abstract

Electrochemical behavior of $La_{0.8}Sr_{0.2}FeO_3$ (LSF) electrode with different porosities under cathodic and anodic current polarization has been investigated by electrochemical impedance spectroscopy and the galvanostatic method. The activation and degradation behavior of the LSF electrode may be related to the partial reduction and oxidation of the Fe ions under cathodic and anodic polarization, especially in the LSF electrodes with high porosities. The performance of the LSF electrode has been found to depend on the oxygen vacancies at the LSF surface, which would promote the transport of oxygen intermediate species at the LSF surface close to the triple-phase boundary (TPB) region. Results show that the polarization resistance (*Rp*) of the LSF electrode decreases at the beginning with the increase of cathodic polarization time, while *Rp* always increases with the increase of anodic polarization time. The effect of cathodic and anodic polarization becomes predominant with the increasing of the porosities of the LSF electrode, which is ascribed to the decrease of the interface area between electrode and electrolyte.

Keywords: B. Porosity; C. Impedance; E. Electrodes; Degradation

1. Introduction

Sr-doped $LaFeO_3$ ($La_{1-x}Sr_xFeO_3$, LSF) has been widely studied for decades as a cathode for solid oxide fuel cells (SOFC) and an anode for steam electrolysis in solid oxide electrolysis cells (SOEC), primarily due to its relatively high conductivity [1,2], high electrocatalytic activity for O^{2-} oxidation and O_2 reduction, and good thermal and chemical compatibility with Y_2O_3-stabilized ZrO_2 (YSZ) electrolyte [3–5].

To improve the electrochemical efficiency, transport related losses due to either mass transport or charged species conduction as well as kinetics-related losses due to charge-transfer and chemical processes must be minimized [6]. However, the cathode in SOFC and the anode in SOEC are thought to be a major contributor to the performance loss in the whole cell [7–9]. The most characteristic behavior of electrodes is the performance enhancement under cathodic polarization. It has been frequently reported that the performance of $La_{1-x}Sr_xMnO_3$ (LSM) and $La_{1-x}Sr_xCo_{1-y}Fe_yO_3$ (LSCF) was improved greatly with time from the onset of cathodic current loading to several hours [10–14]. However, the performance of the porous LSF electrode with high porosities under cathodic and anodic polarization was seldom reported.

Thus, in this study, the electrochemical behavior of the LSF electrode with different porosities under cathodic and anodic polarization was investigated. The origin of the activation and degradation behavior of the LSF electrode under cathodic and anodic polarization was discussed, respectively. In addition, the response of electrodes with

*Corresponding authors. Tel.: +86 10 80194055; fax: +86 10 89796022.
E-mail addresses: wangjing99@gmail.com, wjing09@mails.tsinghua.edu.cn (J. Wang), changsheng@mail.tsinghua.edu.cn (C. Deng).

0272-8842/$ - see front matter © 2012 Elsevier Ltd and Techna Group S.r.l. All rights reserved.
http://dx.doi.org/10.1016/j.ceramint.2012.12.027

different porosities under cathodic and anodic polarization was interpreted by the method named differential analysis of impedance spectra (DIS) [15], which is based on the change that occurs in an impedance spectrum when an optional operation parameter such as polarization time, temperature, etc., is changed.

2. Experimental

2.1. Synthesis of perovskite powders

Analytical grade $Fe(NO_3)_3 \cdot 9H_2O$, $La(NO_3)_3 \cdot 6H_2O$, $Sr(NO_3)_2$ and $C_6H_8O_7$ were used as raw materials to prepare $La_{0.8}Sr_{0.2}FeO_3$ by the self-propagating high-temperature (combustion) synthesis (SHS) method [16]. According to the stoichiometric composition reactants, specified amounts of $Fe(NO_3)_3 \cdot 9 \cdot H_2O$, $Sr(NO_3)_2$ and $La(NO_3)_3 \cdot 6 \cdot H_2O$ were first dissolved in citric acid solution. The molar amount of citric acid was equal to total molar amount of metal nitrates in solution. Ammonia water was slowly added to adjust the pH to 7 and stabilize the nitrate–citrate sol. During this procedure, the solution was continuously stirred and kept at a temperature of 60 °C. Then, the stabilized nitrate–citrate sol was poured into a tray and heated slowly to 130 °C. Viscosity and color changed as the sol turned into a brown, puffy, and porous dry gel. If heated to 170 °C, the dried gel burned completely into loose powders, known as as-synthesized powders. These powders were treated at 900 °C to make the incompletely combusted part react thoroughly. The target perovskite oxide powders were finally obtained.

2.2. Preparation of porous LSF electrodes and the three-electrode system

Three-electrode setup was used to measure the electrochemical performance of porous LSF electrode. Electrode powders were prepared by mixing the desired quantities of LSF powders with pore former. The starch was used as the pore former at the weight fractions of 10, 15, and 20 wt%. These electrode powders were mixed in organic solvent and ball-milled for at least 6 h. Then, the electrode slurries were obtained. The slurries were screen printed onto sintered YSZ discs with a thickness of 0.5 mm and a diameter of 19 mm. In order to obtain a desired electrode thickness of about 20 μm, four layers of the electrode were deposited. Between each deposition, the layers were dried at 170 °C to evaporate the solvent. The samples were then sintered at 1150 °C for 2 h in air to form the porous electrode. Then, half-cells with three kinds of porosities were prepared. Subsequently, Pt paste (PE-Pt-7840, Sino-Platinum Co., Ltd.) was painted onto the other side of the YSZ electrolyte disc as the counter electrode (CE) and also painted as a ring around the CE as the reference electrode (RE). The gap between the CE and the ring RE was 4 mm. Pt wires were stuck on the porous anode, the RE and the CE, followed by baking at 850 °C for 20 min in air. The electrochemical behavior of the LSM electrode under cathodic polarization was investigated with an applied cathodic current of 100 mA cm^{-2} or an anodic current of 100 mA cm^{-2}. The polarization was interrupted from time to time to carry out the measurement of impedance spectroscopy. After the electrode polarization trends became stable, the impedance measurement was carried out after cathodic and anodic polarization treatments.

2.3. Characterization

The phase purity of the LSF powders and the LSF electrode was checked by an X-ray diffractometer (D8 Advance, BRUKER Corporation, Germany). A scanning electron microscope (FESEM, QUANTA 200F, FEI Company, Netherlands) was employed to study the microstructure characteristics of the LSF electrodes. The porosities of the samples were measured by the Archimedes method [17]. To ensure water saturation, the samples were immersed in boiling water for 4 h and allowed to cool in water before weighing. Specific surface area was derived from nitrogen adsorption/desorption isotherms obtained at −196 °C (Micromeritics TriStar II 3020 surface area analyzer). Samples were degassed overnight at 200 °C. The BET theory was used to calculate the surface area of the samples from the linearized BET equation.

All electrochemical measurements were carried out in a program-controlled furnace by an electrochemical impedance spectrometer (SOLARTRON, AMETEK Co., Ltd.) in a frequency range of 0.1–100 kHz under an open-circuit state with a signal amplitude of 10 mV. The electrochemical measurements for the LSF electrodes were conducted at 750 °C which is suitable for high temperature steam electrolysis. The initial and stable electrode behavior of freshly prepared LSF electrodes with cathodic/anodic current passage was studied against the Pt air reference electrode by galvanostatic current interruption (GCI) and electrochemical impedance spectroscopy (EIS) techniques.

Polarization behavior of the LSF electrodes was studied with a constant current density of ± 100 mA cm^{-2}, supplied by a potentiostat/galvanostat (Solartron 1287). After each polarization, the samples were kept at the open-circuit state for 30 min. The polarization was interrupted from time to time to carry EIS measurements. The initial impedance was measured after cathodic/anodic polarization for specified time intervals. The potential of electrode was measured against the Pt reference electrode exposed to air. It was confirmed that the performance of reference electrode did not change during polarization. EIS measurements were performed on the LSF electrodes to investigate the electrochemical behavior of the impedance after cathodic/anodic polarization.

X-ray photoelectron spectroscopy (XPS) analyses were performed on a Thermo Fisher Scientific ESCALAB 250Xi instrument using a monochromatic Al Kα X-ray source (energy 1786.6 eV). A Shirley background was applied. All measured binding energies were charge corrected to the

principal C 1s photoelectron line at 284.6 eV. The XPS analysis was performed at ambient temperature and at pressures typically on the order of $< 10^{-8}$ Torr. Prior to analysis, the samples were outgassed under vacuum for 4 h. The Fe 2p spectra were deconvulated to deduce the Fe^{2+}/Fe^{3+} at the interface between the LSF electrode and the YSZ electrolyte.

3. Result and discussion

3.1. Powder characteristics

The X-ray diffraction patterns of the LSF powders (a) and the LSF|YSZ half-cell (b) are shown in Fig. 1. The XRD patterns of the LSF powders indicate that only characteristic peaks of $La_{0.8}Sr_{0.2}FeO_3$ phase were observed. The result shows that such a perovskite-type oxide can be synthesized at a relatively low temperature (900 °C) by the SHS method. The XRD patterns of LSF|YSZ half-cell indicate that LSF had not reacted with YSZ or decomposed during sample preparation, indicating good chemical compatibility between YSZ and LSF.

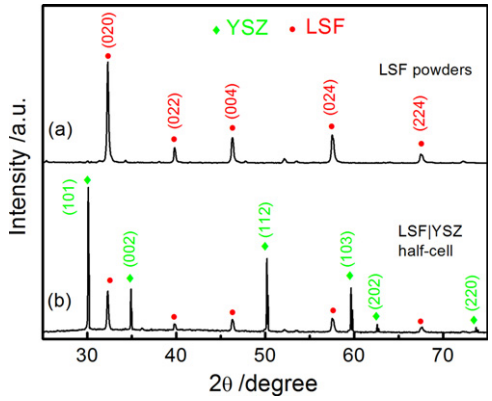

Fig. 1. XRD patterns of the LSF powders (a) and the porous LSF electrodes (b) which were prepared by the self-propagating high-temperature combustion synthesis method and the screen printing method, respectively.

3.2. Microstructural analysis

Fig. 2 shows cross-sectional SEM images of the LSF electrodes with different porosities. It is found that the pores were uniformly distributed over the electrodes. All the samples are highly porous with very uniform particle size distributions, as shown in the insets in Fig. 2(a)–(c). These insets show more details of the electrode morphology at high magnifications and the grain size and pore size can be observed obviously. However, the pore dimensions clearly change in a regular manner with the quantities of the pore former used in the preparation of the ceramic. As shown in Fig. 3(a), the porosity of the electrodes increases with the increase of the pore former content. Rational porosity is an important parameter for the triple-phase boundary (TPB) of electrode because a larger porosity affects the formation of TPB. While the porosities

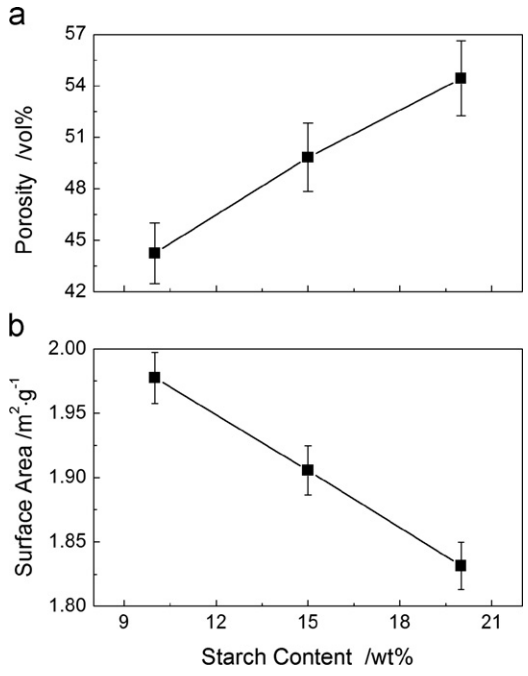

Fig. 3. (a) Relationship between the porosity and the content of pore former, and (b) relationship between the surface area and the content of pore former.

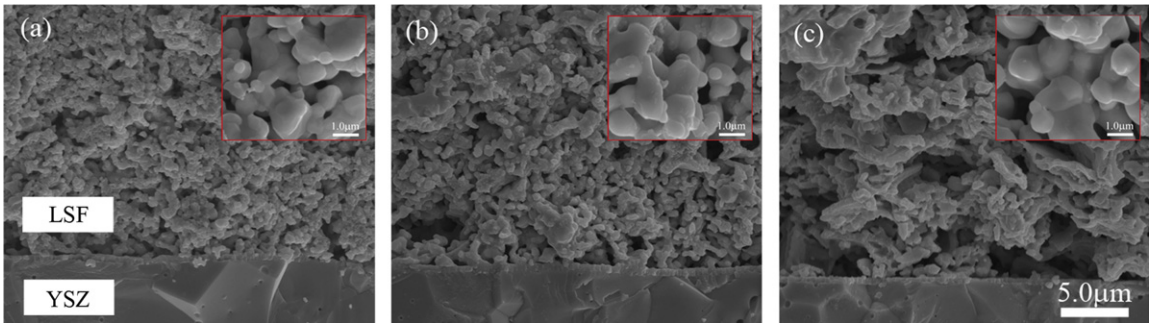

Fig. 2. SEM micrographs of the LSF electrodes with the porosity of (a) 44 vol%, (b) 50 vol%, and (c) 55 vol%.

of the electrodes increased from 43 to 54 vol% by increasing the amount of pore former from 10 to 20 wt% with the same mass of LSF powders, the thickness of the electrode layer was nearly unchanged. However, the bulk conductivity reduced with the increase of the porosity. The surface area was calculated from the data of N_2 adsorption isotherms, as shown in Fig. 3(b). The surface area decreases with the increase of the pore former content. It is due to an increased level of the pore former in a sample preparation that leads to a higher porosity and, as a consequence, a lower value of final surface area.

Though it is difficult to measure exact contact areas of the YSZ electrolyte with the porous LSF electrode, the contact area between LSF and YSZ has been observed by examining the cross section of the porous LSF electrode and could be roughly estimated. As the porosity increases, the contact area between the porous LSF electrode and the YSZ electrolyte correspondingly decreases if the porosity is distributed evenly throughout the LSF electrode.

3.3. Electrochemical performance of the half cells

Fig. 4 shows the impedance spectra of the LSF electrodes with different porosities before and immediately after cathodic and anodic polarization. The impedance behavior of the porous LSF electrodes after cathodic and anodic polarization was compared, as shown in Fig. 4(a), (c), (e) and Fig. 4(b), (d), (f), respectively. The ohmic resistance (*Rs*, the first point of impedance spectroscopy which is intercepted by the *x*-axis in the complex plane) remained nearly unchanged throughout this measurement. The original impedance spectrum consisted of a single depressed semicircle in the complex plane. The *Rp*, which was defined as the distance between the *x*-intercepts of semicircle, was greatly decreased or increased after polarization.

In principle, the impedance response from different processes can be distinguished by EIS. However, if two processes have similar time constants or if there are two parallel reaction pathways, their impedance responses overlap and analysis assuming a single rate-determining step might be invalid. In addition, for a parallel pathway mechanism, the concept of a single rate-determining step being the most resistive step does not apply because the net rate is dominated by the least resistive pathway. Furthermore, most of the simple models used to determine the theoretical reaction order ignore the distributed nature of the porous electrode, which is the spatial variation in potential or species concentration [6]. For visualization at which frequencies two impedance spectra differ from each other, the method of DIS was employed to resolve the impedance spectrum, which makes it possible to selectively

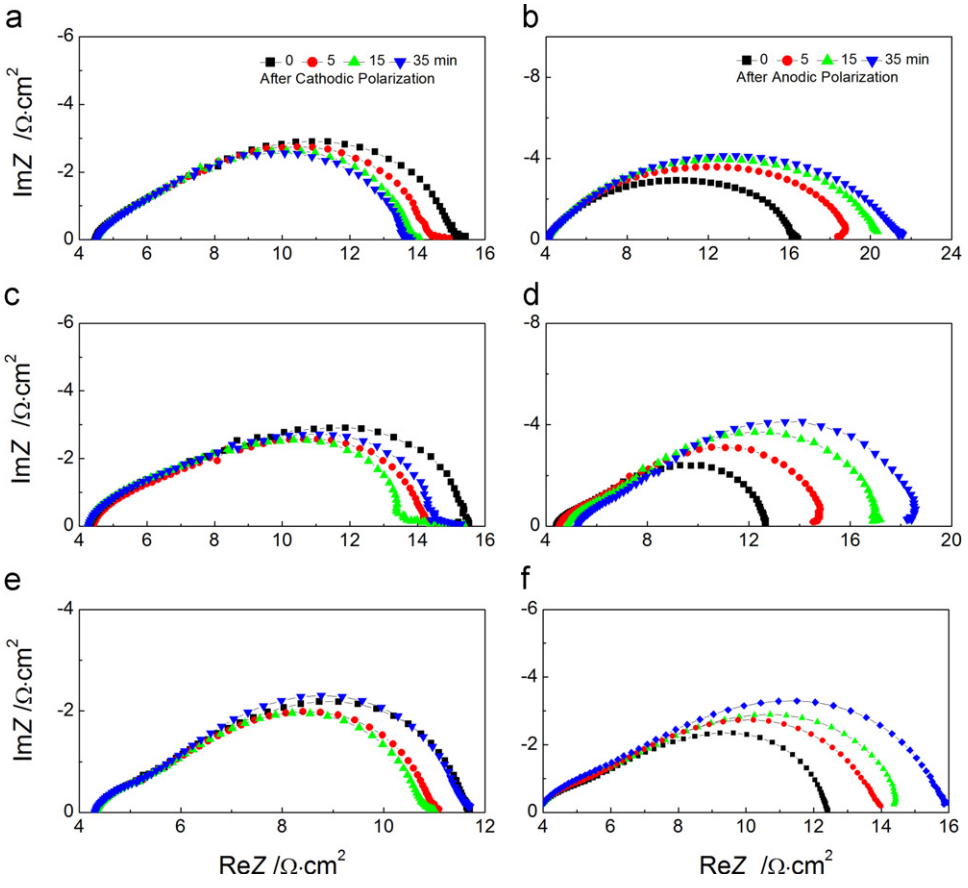

Fig. 4. Changes in impedance spectra of the LSF electrodes with different porosities under cathodic and anodic polarization. (a,b) 44 vol%, (c,d) 50 vol%, (e,f) 55 vol%; (a,c,e) under cathodic polarization, (b,d,f) under anodic polarization.

detect elements contributing in the impedance spectrum where the contribution may be hidden in overlapping contributions from other elements [15].

This technique was applied on a half-cell and the produced DIS obviously revealed three separable parts for the porous LSF electrodes, as shown in Fig. 5. It should be noted that the cathodic/anodic current treatment has negligible effect on the resistance of the high-frequency arc but has significant effect on that of the low-frequency arc for the impedance spectra of the LSF electrode. Especially, dramatic changes appear at low frequency in the electrodes with high porosities as shown in Fig. 5(e) and (f). The high-frequency arcs are attributed to the charge-transfer process, such as O^{2-} transferring from TPB to YSZ under cathodic polarization and from YSZ to TPB under anodic polarization. The low-frequency arcs are commonly associated with surface diffusion of oxygen at the surface of LSF.

The *Rp* reduced under cathodic polarization at the beginning, and with the increase of the polarization time, *Rp* increased, especially in the electrode with high porosities, as shown in Fig. 5(a), (c) and (e). It is known that the oxygen vacancies at the electrode surface extend the active reaction area [18], therefore, surface diffusion of the oxygen vacancies at the LSF surface extends the active reaction sites to the LSF surface for the electrochemical reaction of oxygen under a high cathodic current. As the contact area of interface between the electrode and electrolyte decreases with increasing porosity, the density of polarization current is correspondingly increased as well. Then the effect of activation under cathodic polarization becomes predominant with the increase of the porosity. However, due to the relatively low ionic conductivity of the LSF electrode, the extension of the active sites is markedly limited. Then the *Rp* no longer decrease or even increases gradually as the polarization time is extended.

Theoretically, ferrite is the only redox active element in LSF and hence the only element, which is expected to be significantly affected by cathodic and anodic polarization. Cathodic polarization, which corresponds to a lower oxygen partial pressure will reduce the mean valence state of ferrite and increase the concentration of Fe^{2+}. When the cathodic polarization is negative enough, Fe ions may also be electrochemically reduced with a concomitant generation of oxygen vacancies. Three possible electroredox reactions involved in the LSF electrode under polarization are summarized, as shown in Eqs. (1), (2) and (3). Considering the experimental conditions in this study, the LSF electrode is oxygen-excess at the initial stage, which involves the formation of cation vacancies, as shown in Eq. (4). Combining Eqs. (2) and (4), the reduction of Fe ions at the first stage of cathodic polarization can be

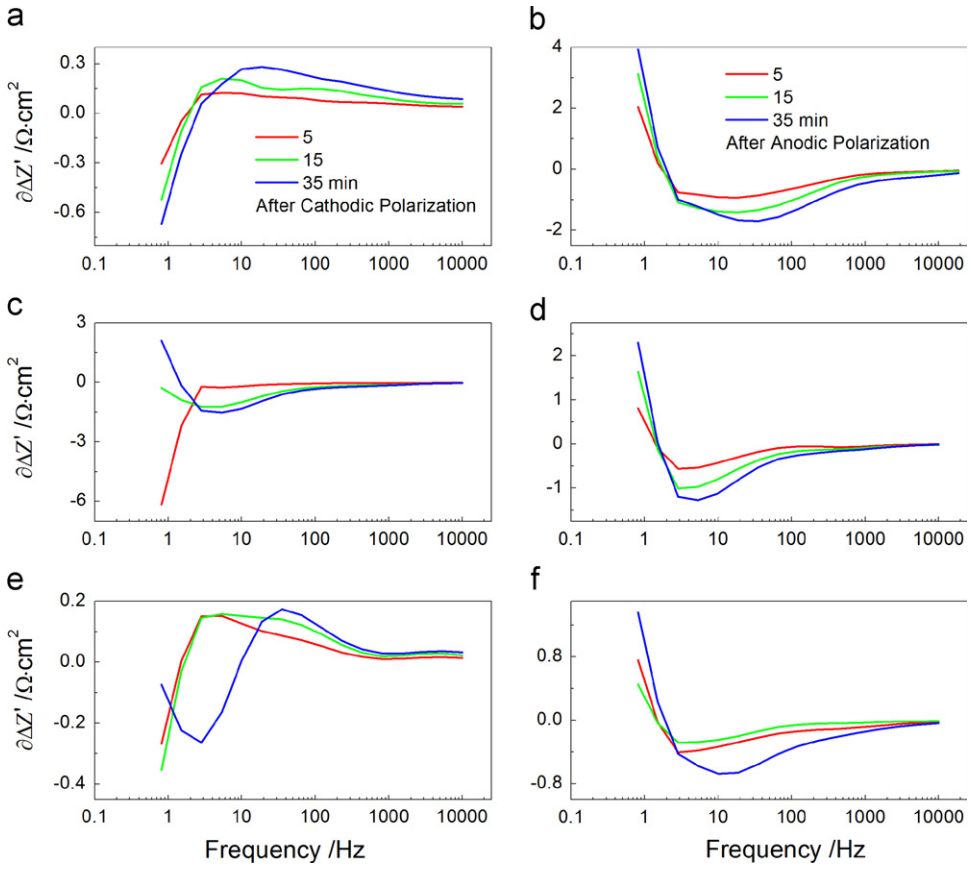

Fig. 5. Changes in DIA of the LSF electrodes with different porosities under cathodic and anodic polarization: (a,b) 44 vol%, (c,d) 50 vol%, (e,f) 55 vol%; (a,c,e) under cathodic polarization, (b,d,f) under anodic polarization.

written as Eq. (5):

$$V_{O,LSF}^{\bullet\bullet} + O_{ad,LSF} + 2e^- \leftrightarrow O_{O,LSF}^{\times} \quad (1)$$

$$O_{O,LSF}^{\times} + 2Fe_{Fe}^{\bullet} + V_{O,YSZ}^{\bullet\bullet} + 2e^- \leftrightarrow V_{O,LSF}^{\bullet\bullet} + 2Fe_{Fe}^{\times} + O_{O,YSZ}^{\times} \quad (2)$$

$$O_{O,LSF}^{\times} + 2Fe_{Fe}^{\times} + V_{O,YSZ}^{\bullet\bullet} + 2e^- \leftrightarrow V_{O,LSF}^{\bullet\bullet} + 2Fe_{Fe}^{\prime} + O_{O,YSZ}^{\times} \quad (3)$$

$$\text{nil} \leftrightarrow V_{La}^{\prime\prime\prime} + V_{Fe}^{\prime\prime\prime} + 3V_{O,LSF}^{\bullet\bullet} \quad (4)$$

$$V_{La}^{\prime\prime\prime} + V_{Fe}^{\prime\prime\prime} + 3O_{O,LSF}^{\times} + 6Fe_{Fe}^{\bullet} + 3V_{O,YSZ}^{\bullet\bullet} + 6e \leftrightarrow 6Fe_{Fe}^{\times} + 3O_{O,YSZ}^{\times} \quad (5)$$

Similar to the oxygen vacancies, Fe ions are also mobile. Therefore, under the cathodic polarization conditions, Fe ions could migrate from the LSF electrode surface to the YSZ electrolyte surface, dissolve in the YSZ electrolyte and diffuse along the YSZ electrolyte surface. During the cathodic polarization, Fe ions in the LSF tend to be reduced. The reduction of $Fe_{Fe}^{\bullet}$ to $Fe_{Fe}^{\times}$ with the concomitant removal of the metal vacancies occurs at the initial stage of the cathodic polarization. The electrical neutrality of LSF is compensated by the formation of oxygen vacancies, which can be described by reaction as shown in Eqs. (2) and (3). Under short-term cathodic polarization, small levels of ferrite were diffused at the electrolyte surface. Under long-term cathodic polarization, ferrite was reduced to an oxidation state of Fe^{2+} and enriched at the electrolyte surface. High concentrations of ferrite firstly appeared at the interface between the electrode and the electrolyte, and then rapidly spread from the TPB over the entire electrolyte surface. Under larger cathodic current passing through the interface between the electrode and the electrolyte in the electrodes with higher porosity, the surface diffusion of ferrite ions at the electrolyte surface was very fast. The rate of such direct incorporation of oxygen into the electrolyte is limited by the electrical conductivity of the surface. Theoretically, the cathode polarization induces a change in electrode surface oxidation state [19]. Under increasingly negative bias, ferrite underwent a continuous reduction from its surface oxidation state. Long-term operation with high cathodic current passing through the electrode and thus removal of Fe from the TPB and the LSF/YSZ interface will lead to an increasing thickness of the Fe deficient LSF layer at the LSF/YSZ interface. Cathodic polarization results in a higher concentration of Fe^{2+} at the LSF/YSZ interface and TPB. The Fe^{2+} has been shown to spread out on the YSZ electrolyte surface. However, with the increase of the polarization time, the removal of Fe^{2+} is greatly enhanced. This will eventually cause a decomposition of LSF at the LSF/YSZ interface. The depletion of Fe will eventually lead to a decomposition of LSF at the LSF/YSZ interface. This causes permanent morphological changes, thereby loss of LSF/YSZ contact and an increase in *Rp*, hence changes of the remaining cathode parameter values, i.e. the parameters of the high and the low frequency cathode arcs as observed from the impedance data, as shown in Fig. 4(c) and (e). The vibrations of $\partial\Delta Z'$ are more obvious at low frequency, as shown in Fig. 5(c) and (e).

The impedance resistance increases with the increase of anodic treatment duration, as shown in Fig. 5(b), (d) and (f). Similar to the effect of the cathodic current treatment, the anodic current treatment also influences the low-frequency arc only, and has almost no effect on the high frequency arc. The ohmic resistance of the electrolyte remains unchanged under the anodic current treatment, which indicates that the interfacial morphology of the LSF electrode remains stable after short-term anodic polarization. Anodic polarization will enhance the oxygen activity at the O_2/LSF/YSZ interface and thus decrease the low oxygen vacancy concentration of LSF, as shown in Fig. 6(b). The reduction of $Fe_{Fe}^{\times}$ to $Fe_{Fe}^{\prime}$, and concomitant generation of oxygen vacancies would promote the transport of oxygen ions at the LSF surface. And the oxidation of $Fe_{Fe}^{\prime}$ to $Fe_{Fe}^{\times}$ then to $Fe_{Fe}^{\bullet}$ would consume the oxygen vacancies, and finally limit the surface diffusion of oxygen ions at the LSF surface. The results of this study also indicate that the low-frequency arc contributing to the O_2 surface diffusion decreases abruptly under a cathodic current treatment. The *Rp* increases sharply under an anodic current. This may be due to oxidation of $Fe_{Fe}^{\prime}$ to $Fe_{Fe}^{\times}$ finally to $Fe_{Fe}^{\bullet}$.

The Electron Spectroscopy for Chemical Analysis (ESCA) results are shown in Fig. 6. Obvious Fe^{3+} peaks were seen for all of the samples (the peaks at binding energies of 724.6 and 711.0 eV can be ascribed to Fe^{3+} [20,21]) after anodic polarization for 35 min, as shown in Fig. 6(b). However, after cathodic polarization for 35 min, the Fe^{2+} peaks (the peaks at binding energies of 722.6 and 709.0 eV can be ascribed to Fe^{2+} [20,21]) had become distinct, as shown in Fig. 6(a). Based on the above results, it is concluded that the mean valence state of ferrite is

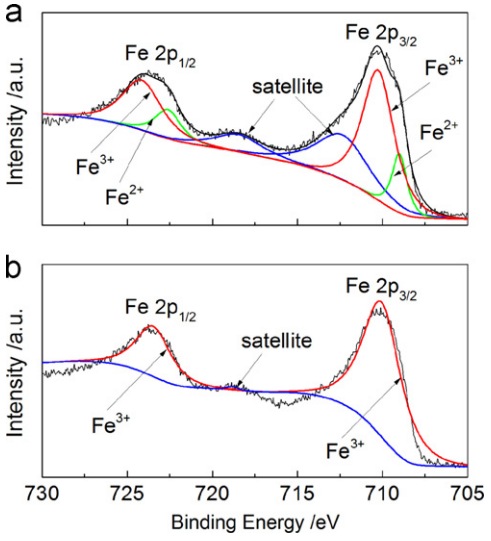

Fig. 6. ESCA spectra of LSF electrode after cathodic polarization (a) and anodic polarization (b).

decreasing and the concentration of Fe^{2+} is increasing after the cathodic polarization. Moreover, the fitted result testifies that there was a relatively high Fe^{3+} concentration at the interface between the LSF and YSZ after the cathodic polarization.

Based on the researches on porous $La_{1-x}Sr_xMnO_3$ electrode in SOFC [19,22,23], three pathways of bulk, surface and interface diffusion of the ionized species are presented in the LSF system, as shown in Fig. 7. Cathode polarization expressed in terms of the corresponding change in oxygen activity shifts the arrow upward (anodic polarization) or downward (cathodic polarization) in the figure. The electrode surface path includes oxygen gas diffusion, adsorption/desorption of oxygen on the electrode surface, diffusion of (possibly dissociated and partly ionized) oxygen species along the surface toward the TPB. The bulk path consists of oxygen gas diffusion, adsorption/desorption on the LSF electrode surface, dissociation and ionization, incorporation into the LSF electrode, oxide ion transport through the electrode and the electrolyte. The electrolyte surface path includes oxygen gas diffusion, adsorption, and ionization on the electrolyte surface (with electrons being provided by the electrolyte), followed by a direct incorporation into the electrolyte. The very low electronic conductivity of YSZ can be expected to restrict the active zone to a region very close to the TPB. Obviously, these three pathways are correlated with the three separable parts in DIS.

The activation and degradation process have been studied generally as part of the mechanism and kinetic studies of the oxygen reduction/oxidation reaction. The activation process in LSF-based electrodes is based on the formation of oxygen vacancies in the LSF under cathodic polarization. The impedance results show that the electrochemical behavior of the LSF electrode seems to be reversible under cathodic and anodic current treatment for short-term polarization. These phenomena could be related to the partial reduction or oxidation of Fe ions under cathodic and anodic polarization, respectively. The appearance of oxygen vacancies at the LSF surface leads to the extension of active area for oxygen incorporation and the promotion of migration of oxygen ion in bulk, thus, the performance can be improved. When the current is interrupted, oxygen vacancies generated during cathodic polarization are consumed by oxidation with gaseous oxygen.

4. Conclusions

The electrochemical behavior of the LSF electrodes with different porosities under cathodic and anodic polarization was investigated by EIS. The *Rp* of the newly prepared LSF electrodes were found to decrease under cathodic current treatment, and subsequently increases when subjected to long-term cathodic polarization. However, the *Rp* was always increased when the LSF electrodes subjected to

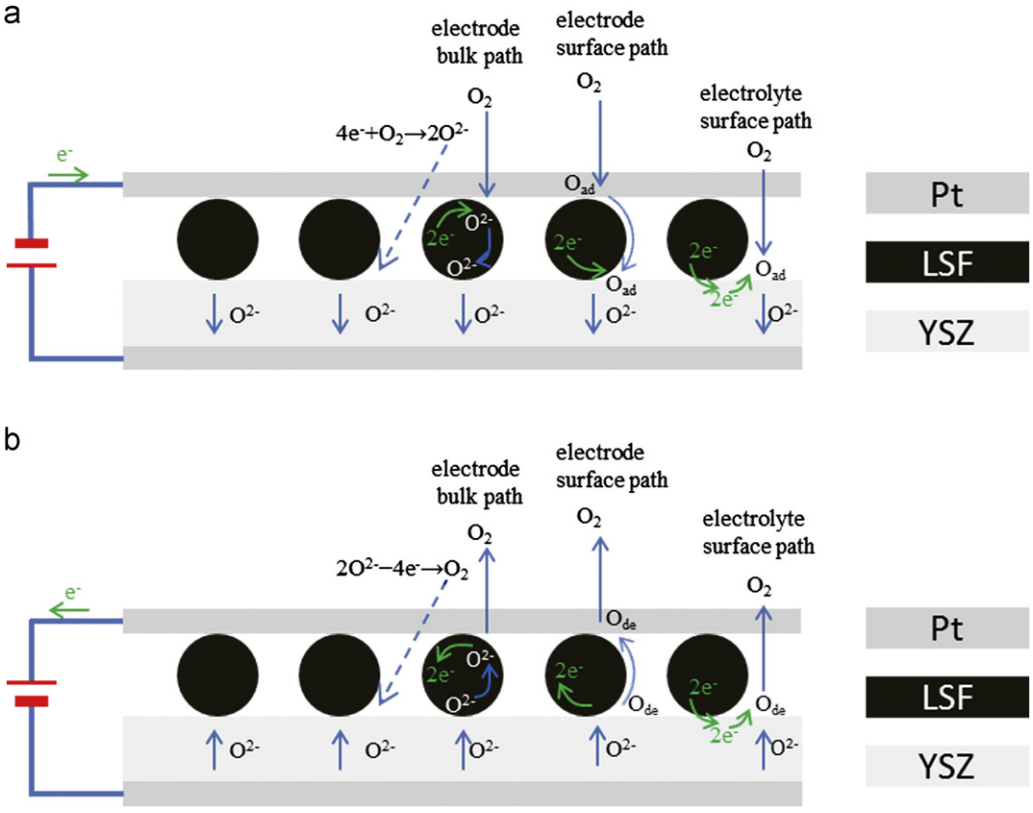

Fig. 7. Schematic presentation of the oxygen incorporation mechanism in the LSF electrodes under cathodic (a) and anodic (b) polarization.

anodic current treatment. The current treatment on LSF electrode only influences the low frequency arc and has negligible effect on the high frequency arc, especially in the electrodes with high porosity.

Acknowledgments

This work was supported by the major project of National Science and Technology (2010ZX06901-020) and the Beijing Natural Science Foundation (2122029). Funding from Tsinghua University (Contract number 20101081790) and State Key Lab of New Ceramics and Fine processing (2010THZ08) was also gratefully acknowledged. Analytical Funding from Tsinghua University covers part of analytical cost.

References

[1] W. Wang, Y. Huang, S. Jung, J.M. Vohs, R.J. Gorte, A comparison of LSM, LSF, and LSCo for solid oxide electrolyzer anodes, Journal of the Electrochemical Society 153 (2006) A2066–A2070.

[2] M.V. Patrakeev, J.A. Bahteeva, E.B. Mitberg, I.A. Leonidov, V.L. Kozhevnikov, K.R. Poeppelmeier, Electron/hole and ion transport in $La_{1-x}Sr_xFeO_{3-\delta}$, Journal of Solid State Chemistry 172 (2003) 219–231.

[3] E.V. Tsipis, V.V. Kharton, Electrode materials and reaction mechanisms in solid oxide fuel cells: a brief review, Journal of Solid State Electrochemistry 12 (2008) 1367–1391.

[4] C. Sun, R. Hui, J. Roller, Cathode materials for solid oxide fuel cells: a review, Journal of Solid State Electrochemistry 14 (2010) 1125–1144.

[5] M.D. Anderson, J.W. Stevenson, S.P. Simner, Reactivity of lanthanide ferrite SOFC cathodes with YSZ electrolyte, Journal of Power Sources 129 (2004) 188–192.

[6] B. Kenney, K. Karan, Estimation of chemical and transport processes in porous, stoichiometric LSM cathodes using steady-state polarization and impedance modeling, Journal of the Electrochemical Society 157 (2010) B1126–B1137.

[7] T. Tsai, S.A. Barnett, Effect of LSM–YSZ cathode on thin-electrolyte solid oxide fuel cell performance, Solid State Ionics 93 (1997) 207–217.

[8] J.J. Choi, W. Qin, M. Liu, M. Liu, Preparation and characterization of $(La_{0.8}Sr_{0.2})_{0.95}MnO_{3-\delta}$ (LSM) thin films and LSM/LSCF interface for solid oxide fuel cells, Journal of the American Ceramic Society 94 (2011) 3340–3345.

[9] R. Knibbe, M.L. Traulsen, A. Hauch, S.D. Ebbesen, M. Mogensen, Solid oxide electrolysis cells: degradation at high current densities, Journal of the Electrochemical Society 157 (2010) B1209–B1217.

[10] Y. Tao, H. Nishino, S. Ashidate, H. Kokubo, M. Watanabe, H. Uchida, Polarization properties of $La_{0.6}Sr_{0.4}Co_{0.2}Fe_{0.8}O_{3-\delta}$ based double layer-type oxygen electrodes for reversible SOFCs, Electrochimica Acta 54 (2009) 3309–3315.

[11] J. Yang, H. Muroyama, T. Matsui, K. Eguchi, A comparative study on polarization behavior of (La,Sr)MnO_3 and (La,Sr)CoO_3 cathodes for solid oxide fuel cells, International Journal of Hydrogen Energy 35 (2010) 10505–10512.

[12] J. Yang, H. Muroyama, T. Matsui, K. Eguchi, Simulation of dynamic response of strontium-doped lanthanum manganite under cathodic polarization, Journal of the Electrochemical Society 157 (2010) B449–B454.

[13] S.P. Jiang, Activation, microstructure, and polarization of solid oxide fuel cell cathodes, Journal of Solid State Electrochemistry 11 (2007) 93–102.

[14] X.J. Chen, K.A. Khor, S.H. Chan, Electrochemical behavior of La(Sr)MnO_3 electrode under cathodic and anodic polarization, Solid State Ionics 167 (2004) 379–387.

[15] S.H. Jensen, A. Hauch, P.V. Hendriksen, M. Mogensen, N. Bonanos, T. Jacobsen, A method to separate process contributions in impedance spectra by variation of test conditions, Journal of the Electrochemical Society 154 (2007) B1325–B1330.

[16] H.C. Yi, J.J. Moore, Self-propagating high-temperature (combustion) synthesis (SHS) of powder-compacted materials, Journal of Materials Science 25 (1990) 1159–1168.

[17] M. Boaro, J.M. Vohs, R.J. Gorte, Synthesis of highly porous yttria-stabilized zirconia by tape-casting methods, Journal of the American Ceramic Society 86 (2003) 395–400.

[18] T. Horita, K. Yamaji, M. Ishikawa, N. Sakai, H. Yokokawa, T. Kawada, T. Kato, Active sites imaging for oxygen reduction at the $La_{0.9}Sr_{0.1}MnO_{3-x}$/yttria-stabilized zirconia interface by secondary-ion mass spectrometry, Journal of the Electrochemical Society 145 (1998) 3196–3202.

[19] M. Backhaus-Ricoult, K. Adib, T. Clair St., B. Luerssen, L. Gregoratti, A. Barinov, In-situ study of operating SOFC LSM/YSZ cathodes under polarization by photoelectron microscopy, Solid State Ionics 179 (2008) 891–895.

[20] T. Yamashita, P. Hayes, Analysis of XPS spectra of Fe^{2+} and Fe^{3+} ions in oxide materials, Applied Surface Science 254 (2008) 2441–2449.

[21] A. Chainani, M. Mathew, D.D. Sarma, Electronic structure of $La_{1-x}Sr_xFeO_3$, Physical Review B 48 (1993) 14818–14825.

[22] J. Fleig, Solid oxide fuel cell cathodes: polarization mechanisms and modeling of the electrochemical performance, Annual Review of Materials Research 33 (2003) 361–382.

[23] V. Brichzin, J. Fleig, H.U. Habermeier, G. Cristiani, J. Maier, The geometry dependence of the polarization resistance of Sr-doped $LaMnO_3$ microelectrodes on yttria-stabilized zirconia, Solid State Ionics 152 (2002) 499–507.